# **Faraday Discussions**

Cite this: Faraday Discuss., 2023, 243, 231



**PAPER** 

View Article Online View Journal | View Issue

# A conformational equilibrium in the nitrogenase MoFe protein with an $\alpha$ -V70I amino acid substitution illuminates the mechanism of H<sub>2</sub> formation†

Dmitriy A. Lukoyanov, a Zhi-Yong Yang, b Krista Shisler, c John W. Peters, d Simone Raugei, De Dennis R. Dean, f Lance C. Seefeldt b and Brian M. Hoffman ba

Received 14th November 2022, Accepted 9th January 2023

DOI: 10.1039/d2fd00153e

Study of α-V70I-substituted nitrogenase MoFe protein identified Fe6 of FeMo-cofactor (Fe<sub>7</sub>S<sub>9</sub>MoC-homocitrate) as a critical N<sub>2</sub> binding/reduction site. Freeze-trapping this enzyme during Ar turnover captured the key catalytic intermediate in high occupancy, denoted  $E_4(4H)$ , which has accumulated  $4[e^-/H^+]$  as two bridging hydrides, Fe2-H-Fe6 and Fe3-H-Fe7, and protons bound to two sulfurs.  $E_4(4H)$  is poised to bind/reduce  $N_2$ as driven by mechanistically-coupled H2 reductive-elimination of the hydrides. This process must compete with ongoing hydride protonation (HP), which releases H2 as the enzyme relaxes to state  $E_2(2H)$ , containing  $2[e^-/H^+]$  as a hydride and sulfur-bound proton; accumulation of  $E_4(4H)$  in  $\alpha$ -V70I is enhanced by HP suppression. EPR and  $^{95}$ Mo ENDOR spectroscopies now show that resting-state lpha-V701 enzyme exists in two conformational states, both in solution and as crystallized, one with wild type (WT)-like FeMo-co and one with perturbed FeMo-co. These reflect two conformations of the Ile residue, as visualized in a reanalysis of the X-ray diffraction data of  $\alpha$ -V70I and confirmed by computations. EPR measurements show delivery of  $2[e^{-}/H^{+}]$  to the  $E_{0}$ state of the WT MoFe protein and to both  $\alpha$ -V70I conformations generating E<sub>2</sub>(2H) that contains the Fe3-H-Fe7 bridging hydride; accumulation of another 2[e-/H+] generates  $E_4$ (4H) with Fe2-H-Fe6 as the second hydride.  $E_4$ (4H) in WT enzyme and a minority  $\alpha$ -V70I E<sub>4</sub>(4H) conformation as visualized by QM/MM computations relax to resting-state through two HP steps that reverse the formation process: HP of Fe2-H-Fe6 followed by slower HP of Fe3-H-Fe7, which leads to transient accumulation of  $E_2(2H)$ 

<sup>&</sup>lt;sup>a</sup>Department of Chemistry and Molecular Biosciences, Northwestern University, Evanston, Illinois 60208, USA

<sup>&</sup>lt;sup>b</sup>Department of Chemistry and Biochemistry, Utah State University, Logan, Utah 84322, USA

Institute of Biological Sciences, Washington State University, Pullman, Washington, 99164, USA

<sup>&</sup>lt;sup>d</sup>Department of Chemistry and Biochemistry, University of Oklahoma, Norman, Oklahoma, 73019, USA

Physical and Computational Sciences Directorate, Pacific Northwest National Laboratory, Richland, Washington, 99352, USA

<sup>&</sup>lt;sup>f</sup>Biochemistry Department, Virginia Tech, Blacksburg, Virginia, 24061, USA

<sup>†</sup> Electronic supplementary information (ESI) available. See DOI: https://doi.org/10.1039/d2fd00153e

containing Fe3-H-Fe7. In the dominant  $\alpha$ -V70I E<sub>4</sub>(4H) conformation, HP of Fe2-H-Fe6 is passively suppressed by the positioning of the Ile sidechain; slow HP of Fe3-H-Fe7 occurs first and the resulting E<sub>2</sub>(2H) contains Fe2-H-Fe6. It is this HP suppression in E<sub>4</sub>(4H) that enables  $\alpha$ -V70I MoFe to accumulate E<sub>4</sub>(4H) in high occupancy. In addition, HP suppression in  $\alpha$ -V70I E<sub>4</sub>(4H) kinetically unmasks hydride reductive-elimination without N<sub>2</sub>-binding, a process that is precluded in WT enzyme.

### Introduction

The  $\alpha$ -V70I amino acid substituted nitrogenase MoFe protein has played an important role in studies of the mechanism of nitrogen fixation by nitrogenase. A kinetic scheme of this mechanism is summarized in Fig. 1.<sup>1-3</sup> The reported crystal structure of the  $\alpha$ -V70I variant revealed that the larger isoleucine sidechain, positioned over Fe6 of the active site FeMo-cofactor, impedes substrate access to this iron, thereby explaining suppression of  $N_2$  reduction in the substituted protein and identifying Fe6 as a critical site on the Fe2,3,6,7 face at which  $N_2$  binds.<sup>4,5</sup> Below we present a more detailed reanalysis of that structure.

Freeze-trapping the  $\alpha$ -V70I MoFe protein during turnover under Ar captures an intermediate in high occupancy that was shown by EPR and ENDOR studies to contain two bridging hydrides, Fe2–H–Fe6 and Fe3–H–F7, Fig. 2.<sup>6,7</sup> This intermediate also is freeze-trapped in wild type (WT) enzyme, but in low occupancy.<sup>8</sup> Of particular importance to the present study, the additional protons are bound to the sulfurs that form Fe2–S2B–Fe6 and Fe3–S5A–Fe7 bridges in the resting-state (E<sub>0</sub>) structure,<sup>7</sup> but as will be further discussed below, density functional theory (DFT) computations indicated that the Fe2–SH bond in E<sub>4</sub>(4H) is hemilabile and can cleave to generate an Fe6–SH moiety, Fig. 2.<sup>9</sup>

The  $E_4(4H)$  state has identical physical properties in the WT and  $\alpha$ -V70I MoFe proteins – the same EPR/ENDOR spectra and photolysis characteristics<sup>8</sup> – but its high occupancy when freeze-trapped in the substituted protein makes it particularly favorable for ENDOR study. However, the WT enzyme can also be freeze-trapped in an  $N_2$ -bound state during turnover under  $N_2$ .<sup>10</sup> Cryoannealing

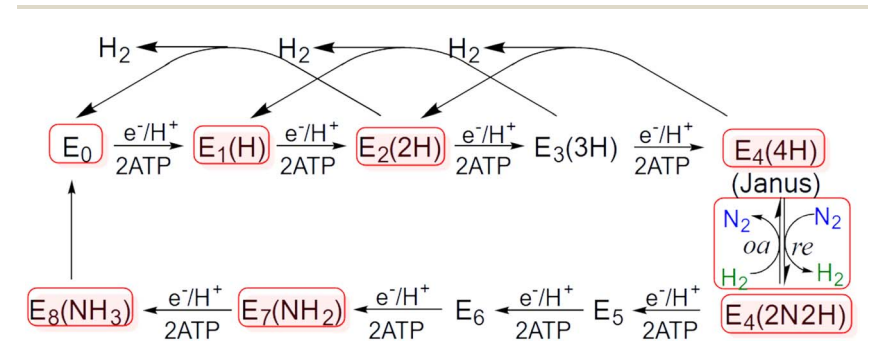


Fig. 1 Simplified  $8[e^-/H^+]$  kinetic scheme for nitrogen reduction. In the Lowe–Thorneley  $E_n$  notation, n= number of  $[e^-/H^+]$  added to FeMo-co; in parentheses, the stoichiometry of H/N bound to FeMo-co. The reductive-elimination/oxidative-addition (re/oa) equilibrium is highlighted in red; and the intermediates in red boxes have been freeze trapped for spectroscopic study.

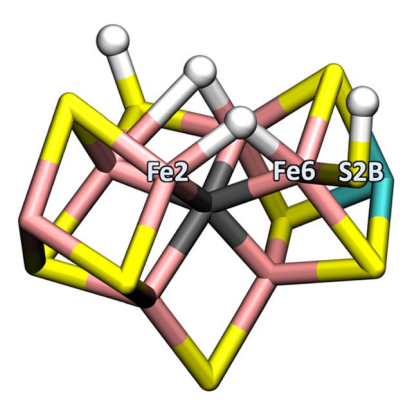


Fig. 2 Structure of  $E_4$ (4H) in WT enzyme showing cleaved Fe2–S2B–H bond as obtained from density functional theory calculations. The FeMo-co atoms are colored as follows: sulfurs in yellow, central carbide in dark gray, irons in rust, and Mo in teal.

experiments with WT enzyme freeze-trapped during turnover under  $N_2$ , combined with similar experiment with the substituted enzyme freeze-trapped during Ar turnover, showed the  $N_2$ -bound state to be  $E_4(2N2H)^{11}$  (Fig. 1) and established the state with two bridging hydrides to be  $E_4(4H)$ . This latter state is the key state in nitrogen fixation, the Janus intermediate that is activated to bind/reduce  $N_2$  with the concerted reductive elimination of  $H_2$ .

As a foundation for understanding the behavior of WT enzyme and the  $\alpha\textsc{-V70I}$  variant, this report begins by showing that both in solution and as crystallized, the  $\alpha\textsc{-V70I}$  variant exhibits two conformational substates. It then examines in detail: (i) what are found to be differing pathways by which WT and  $\alpha\textsc{-V70I}$  variant MoFe proteins accumulate [e $^-/H^+$ ] to form intermediates  $E_2(2H)$  and  $E_4(4H)$  during Ar turnover, and (ii) the pathways by which these intermediates relax to  $E_0$  by  $H_2$  release through HP.

## Materials and methods

The Azotobacter vinelandii strains DJ995, DJ1373, and DJ884 expressing the wild-type (WT),  $\alpha$ -V70I MoFe protein, and the Fe protein, respectively, were grown and the corresponding proteins were prepared and characterized as previously described.<sup>6,13</sup> The samples employed to acquire the EPR and ENDOR spectra presented below are specified in Table S1.†

The  $\alpha$ -V70I, <sup>95</sup>Mo–MoFe protein used for preparation of crystals for EPR measurements was stored in a buffer containing 50 mM Tris, pH 8, 250 mM NaCl, and 2 mM dithionite buffer. Crystals were obtained in about 2 weeks using a microcapillary batch diffusion method, set up under anaerobic conditions in an MBraun anaerobic chamber, as previously described.<sup>5,14</sup> The crystals were harvested in an anaerobic Coy chamber, washed with crystallization buffer (diluted with 50 mM Tris, pH 8, 150 mM NaCl to mimic crystallization conditions), and the slurry was loaded into Q-band tubes and quickly frozen in liquid nitrogen.

X-band EPR spectra were measured on an ESP 300 Bruker spectrometer equipped with an Oxford ESR 900 liquid helium flow cryostat. Obtained spectra

were simulated with EasySpin software.<sup>15</sup> Q-band CW EPR and pulse ENDOR spectra were acquired at 2 K on spectrometers equipped with liquid helium immersion Dewars as described elsewhere.<sup>16,17</sup>

Molecular dynamics (MD) simulations were used to refine the X-ray data of the  $\alpha$ -V70I variant. Simulations were performed using the protocol described in ref. 18 augmented by umbrella sampling to estimate the relative free energy of potential  $\alpha$ -V70I conformations. Quantum chemical calculation based on density functional theory were performed to further refine the structure of the  $E_0$  and  $E_4(4H)$  states. These calculations were performed on truncated models of the catalytic pocket as described in ref. 18 and adopted the BP86 exchange and correlation functional<sup>19-21</sup> and the def2-TZVP basis set<sup>22</sup> for all atoms with the addition of an effective core potential for Mo.<sup>23</sup>

### Results and discussion

#### α-V70I substitution introduces a MoFe protein conformational equilibrium

We compared the frozen-solution EPR and  $^{95}$ Mo ENDOR spectra of the WT and  $\alpha$ -V70I MoFe proteins in the E $_0$  resting state, and further compared the EPR spectrum of  $\alpha$ -V70I in frozen solution with that in crystals. The EPR spectrum of WT E $_0$  resting-state frozen solutions exhibits a single S=3/2 signal, named 1a,  $^{24}$  with measured g'-values relative to a fictitious spin  $S'=\frac{1}{2}$  of g'=[4.33, 3.65, 2.01], and similarly for single crystals.  $^{25,26}$  In contrast, the  $\alpha$ -V70I resting state, both in frozen solution and in a frozen polycrystalline slurry, exhibits EPR signals from two conformers of the FeMo-co with different rhombicity. One has an EPR spectrum with essentially the same g'-values as WT enzyme E $_0$ /1a, while the other has higher rhombicity, with  $g'_1=4.53$  (Fig. 3, left); this perturbed conformation is denoted, E $_0$ /1a'. As seen in Fig. 3, comparable amounts of the two conformers are trapped in frozen solution and in the crystals of the crystalline slurry. However, the relative abundances of the two conformers can vary with sample, which we attribute to the trapping of various non-equilibrium populations.

 $^{95}$ Mo (I=5/2) Davies ENDOR spectra collected at fields where the EPR spectra of the two conformers overlap show distinct  $m_{\rm I}=\pm 1/2$  doublets from the two conformers (Fig. 3, right). Only one doublet is seen at  $g'_1=4.53$ , where only the higher-rhombicity  ${\rm E}_0/1a'$  signal is present. That doublet is centered at  $A'({\rm obs})/2=6.98$  MHz, which corresponds to the hyperfine coupling in the S=3/2 representation of  $A_1=A'({\rm obs})\times(2/g')=6.16$  MHz. This observation of a signal from a single conformer allows assignment of the ENDOR spectra to the appropriate S=3/2 EPR conformer signal where the EPR spectra overlap. At  $g'_1=4.36$  for the WT conformer, its doublet is centered at  $A'({\rm obs})/2=4.98$  MHz and corresponds to  $A_1=4.57$  MHz, essentially the same value previously obtained from  $^{95}$ Mo ENDOR of WT resting state. Thus, the influence on FeMo-co of the perturbation associated with the conformation of the large Ile side chain as seen in the  $E_0$  FeMo-co EPR signal extends to the Mo site of the cofactor.

#### Crystal structure of α-V70I

Encouraged by the finding that the  $\alpha$ -V70I variant exists in two substates, both in crystals and frozen solution, the structure of the  $\alpha$ -V70I variant<sup>5</sup> was revisited. In this structure the electron density maps of the Ile are ambiguous, and we now find

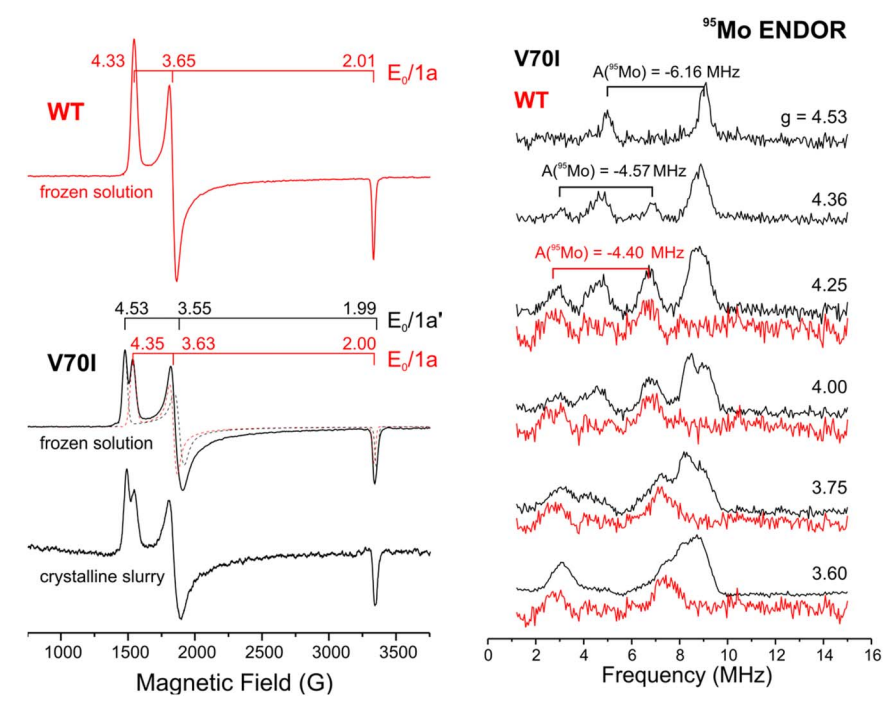


Fig. 3 Left, X-band EPR of frozen solutions of WT and α-V70I MoFe proteins in the  $E_0$  resting state, and of a polycrystalline slurry of the latter; dashed lines are EasySpin simulation deconvoluting the two conformers of the α-V70I solution resting state. Right, Q-band Davies  $^{95}$ Mo ENDOR of the proteins prepared with  $^{95}$ Mo labeling of FeMo-cofactor. Shown  $^{95}$ Mo hyperfine couplings were obtained as described in the text and signed as described in ref. 27. EPR conditions: temperature, 3.8 K; microwave frequency,  $\sim$ 9.36 GHz; microwave power, 0.5 mW; modulation amplitude, 13 G; time constant, 160 ms; field sweep speed, 33 G s<sup>-1</sup>. ENDOR conditions: temperature, 2 K; microwave frequency, 34.78 GHz (α-V70I) and 34.72 GHz (WT); Davies sequence,  $t(\pi/2) = 40$  ns,  $\tau = 600$  ns, RF 40 μs; repetition time, 5 ms; spectra were taken with noise broaden RF bandwidth and 20 MHz RF filter.

the assignment of two conformations at this position, Fig. 4, refines as well, if not better, than the single conformation previously assigned. MD simulations based on empirical force fields also indicate two conformers, separated by a free energy barrier of 40 kJ mol<sup>-1</sup>, with conformer 1 of Fig. 4 being about 5 kJ mol<sup>-1</sup> more stable in free energy than conformer 2. Refinement of the two conformers using DFT confirms this result. The energy difference from the MD simulations yields relative populations of 88% and 12%, but given the uncertainties in relative energies of the two conformers, the computations are compatible with the roughly 1:1 population ratio of the two conformers indicated by both the solution and crystal EPR measurements.

The ethyl arm of the  $\alpha$ -Ile70 sidechain approaches S2B more closely in conformer 1 (3.0 Å) than in the other (4.3 Å), Fig. 4. We propose that conformer 1 corresponds to the perturbed conformer seen spectroscopically, with its g'-shift and  $^{95}$ Mo hyperfine changes for the  $E_0$  state of the variant, and that these differences are caused by the sidechain interactions with FeMo-co, in particular

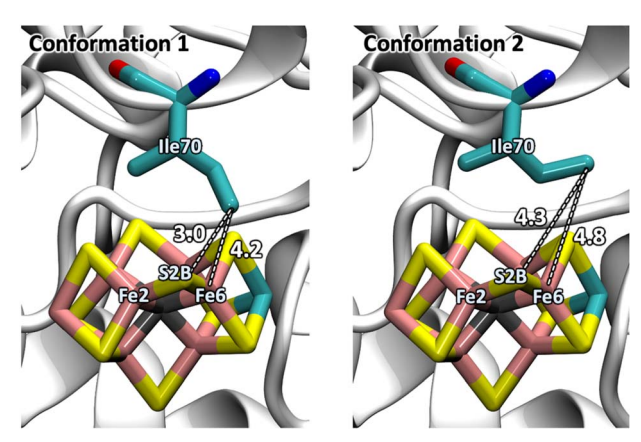


Fig. 4 Refined structure of  $\alpha$ -V70I variant with Ile conformers 1 (left) and 2 (right). Distances (in Å) are shown from the Ile delta carbons to the S2B and Fe6 of the FeMo-co. The FeMo-co atoms are colored as follows: sulfurs in yellow, central carbide in dark gray, irons in rust, and Mo in teal.

with S2B. We further propose that FeMo-co in the other conformer 2 exhibits properties seen in  $E_0$  of the WT enzyme, which thus represents the unperturbed conformer.

#### α-V70I conformational interconversion, N2 reduction and E4(4H) accumulation

The substitution of the  $\alpha$ -V70, which 'sits' over Fe6 of FeMo-co, by isoleucine, with its larger sidechain, causes the specific activity for N2 reduction to 2NH3 to decrease by  $\sim$ 2/3, with an even greater decrease in specific activity for acetylene reduction.4 This effect established that N2 and C2H2 react at Fe6, with the isoleucine sidechain interfering with their access. The observation that the α-V70I variant shows two distinct Eo conformers modulates the interpretation of its decreased specific activity for N2 reduction by suggesting that ambienttemperature turnover likewise involves multiple conformers, and that they have different reactivities. As one possible limiting interpretation, E4(4H) would also exhibit two types of conformers ('two-conformer limit') at ambient temperature, one showing WT reactivity (R conformers), the other with N<sub>2</sub> binding blocked (U conformers). In an opposing limit, at ambient there would be an ensemble of conformational states with a range of degrees of N2 inhibition. In this case, the crystal-structure and solution results would then imply that this ensemble collapses upon cooling/crystallization into two sub-ensembles/conformers. This issue is addressed below in measurements of the kinetics of loss of Eo during lowflux Ar turnover of WT and  $\alpha$ -V70I MoFe protein.

As shown in the kinetic scheme of Fig. 1,  $N_2$  binds to  $E_4(4H)$  with concerted reductive elimination (re) of its two bridging hydrides as  $H_2$ . It is simple to show that if  $E_4(4H)$  exhibits the two-conformer limit at ambient temperature, one showing WT reactivity (R conformer), the other being unreactive (U conformer), then the rate constant for  $N_2$ -binding/reductive-elimination would be reduced by the factor  $s = 1/(1 + K_c)$ , where  $K_c = [U]/[R]$  is the equilibrium ratio between interconverting U and R conformers. The measured  $s \sim 1/3$  during catalytic  $N_2$ 

reduction at ambient temperatures then would imply  $K_c \sim 2$ . These two conformers presumably correspond to the two observed in frozen-solution and crystals of the resting-state enzyme. In the following measurements, we examine conformational contributions to reactivity by examining frozen solutions, and as encouraged by low-flux measurements to be described, discuss them in terms of the two-conformer limit.

Rapid freeze quench and the reaction of reduced Fe-protein with  $\alpha$ -V70I conformers. To test the reactivity of the reduced Fe protein with the  $\alpha$ -V70I conformers, Fe-protein  $\rightarrow \alpha$ -V70I MoFe-protein electron transfer was studied by rapid–freeze–quench (RFQ) techniques, in which solutions of reduced Fe protein (Fe-red) and  $\alpha$ -V70I MoFe were rapidly mixed with ATP to initiate electron transfer, then frozen at predetermined times subsequently: 35, 320, and 1600 ms (Fig. 5). The early-time sample shows that during reduction of  $E_0$   $\alpha$ -V70I MoFe the signals from the two frozen-state conformers decrease in parallel, with roughly 2/3 of each having been reduced by 35 ms while the 1b signal of the  $E_2(2H)$  state appears concomitantly. Thus, the two conformers show the same rate of electron accumulation. The  $E_2(2H)/1b$  signal increases through 320 ms of reaction and then decreases along with further decrease of the  $E_0$  conformer signals in favor of accumulation of the  $E_4(4H)$  state, which appears after 1600 ms (not shown). The

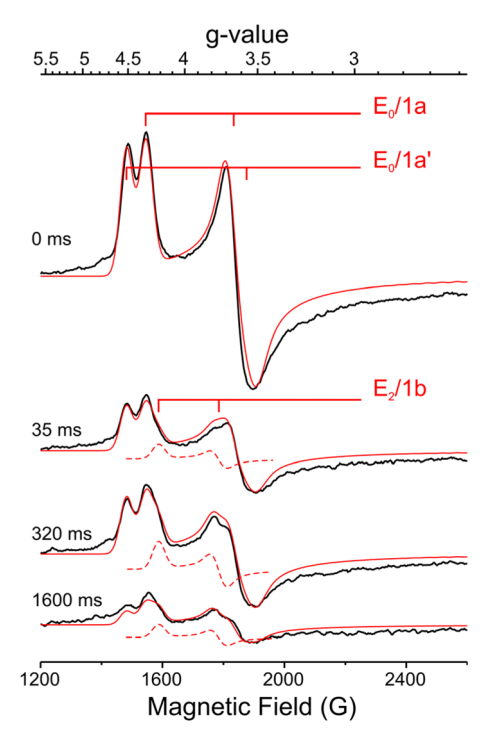


Fig. 5 EPR spectra of rapid freeze quenched samples prepared during  $\alpha$ -V70I Ar turnover under high electron flux (MoFe protein: Fe protein = 1:10). Solid red lines are EasySpin simulations, which are sums of contributions from 1a, 1a', and 1b as discussed in text. Dashed red lines exhibit the contributions of E<sub>2</sub>(2H)/1b. EPR conditions: the same as in Fig. 3.

 $E_4(4H)$  accumulation in  $\alpha$ -V70I is much greater than seen for WT enzyme, indicating that this is associated with the presence of the perturbed  $\alpha$ -V70I conformer  $E_0/1a'$ .

Population estimates of the high spin states obtained as described previously<sup>29</sup> show that in the RFQ time range of 35–320 ms, the combined population of  $E_0/1a$  and  $E_0/1a'$  states decreases to  $\sim$ 40% and stays unchanged, while population of  $E_2(2H)/1b$  accounts for  $\sim$ 20%. This distribution is consistent with populations of  $E_0/1a$  and  $E_2(2H)/1b$  previously observed in similar RFQ experiment for WT enzyme,<sup>30</sup> and is roughly in accordance with prediction of the Lowe and Thorneley kinetic model.<sup>31</sup> Considering that none of the other  $E_2(2H)$  signals discussed below are seen in spectra of RFQ samples, it can be concluded that both  $\alpha$ -V70I conformers –  $E_0/1a$  and  $E_0/1a'$  – form only  $E_2(2H)/1b$  upon two-fold reduction.

Low-flux turnover of WT and  $\alpha$ -V70I; implication for conformational equilibrium and rates of HP at ambient temperatures. Given the above observation that the electron-accumulation is unaffected by the  $\alpha$ -V70I substitutions, the observation of enhanced  $E_4(4H)$  populations with  $\alpha$ -V70I implies that the amino acid substitution decreases the HP rate constant of the perturbed  $\alpha$ -V70I conformation. In confirmation of this conclusion, such a decrease also is observed in turnover measurements at ambient temperatures under extremely low electron flux, which is achieved by mixing MoFe and Fe proteins in very unequal proportions of 100 MoFe per 1 Fe protein. After several minutes of such low-flux turnover of the WT enzyme approximately half the cofactors of the WT enzyme are reduced, Fig. 6, yet EPR spectra show no noticeable traces of  $E_2(2H)/1b$  (or  $E_4(4H)$ ), indicating that the 'missing'  $E_0$  resting state has been reduced to the EPR-silent state  $E_1(H)$ . In short, the WT nitrogenase had reached a steady-state equilibrium involving only the two states,  $E_0$ ,  $E_1(H)$ . This arises because under this low-flux condition, electron delivery to cofactor in WT enzyme is too slow to

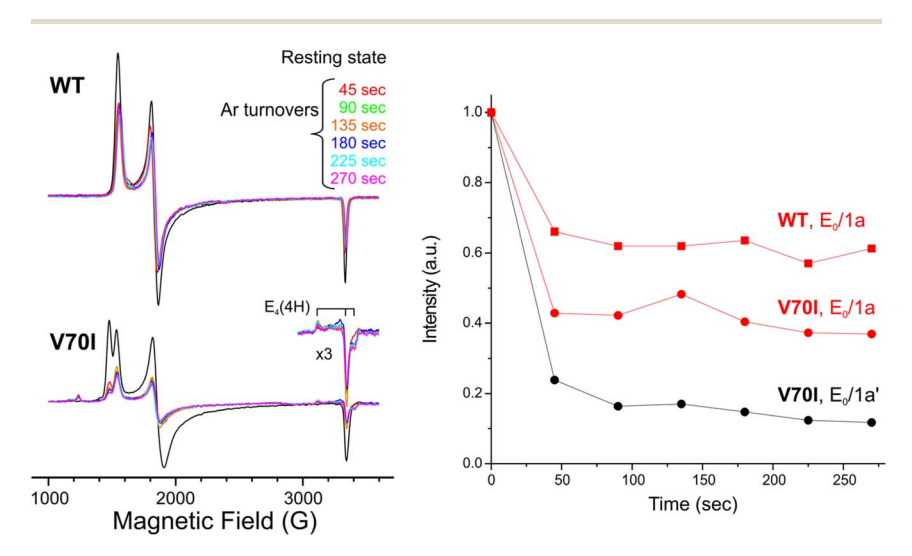


Fig. 6 Left, EPR spectra of low electron flux MoFe protein: Fe protein = 100:1 turnover samples prepared with WT and  $\alpha$ -V70I MoFe proteins. Right, decrease of the resting state populations with time of turnover; the data points were obtained as  $g_1$  feature amplitude for the indicated S = 3/2 EPR-active states. EPR conditions: the same as in Fig. 3.

compete with HP at the  $E_2(2H)$  state. Once a second electron/proton is delivered to  $E_1(H)$  to form  $E_2(2H)$ ,  $H_2$  generation by HP and its release outcompetes electron delivery to achieve more-reduced states. Remarkably, this behavior is exactly as predicted by the kinetic scheme of Fig. 1 for low-flux steady state turnover: no matter how small the flux, if steady state is achieved, then states  $E_0$  and  $E_1$  are predicted to have equal populations, 50% of the total.

The low-flux behavior of the  $\alpha$ -V70I variant is dramatically different. As shown in Fig. 6, freeze-trapping α-V70I during low-flux turnover shows that its unperturbed resting state  $E_0/1a$  conformer undergoes the same  $\sim$ 50–60% loss as for WT upon reaching steady state, but the perturbed conformer  $E_0/1a'$  shows an  $\sim$ 90% resting-state loss, accompanied by the appearance of reduced E-states, even including the dihydride  $E_4(4H)$ . In consonance with cryoannealing observations presented below, this shows that the rate constant for HP relaxation of E<sub>2</sub>(2H) for the perturbed conformer is so small that even under such low-flux condition, further reduction of this conformer outcompetes HP in  $E_2(2H)$ , and causes nearcomplete depopulation of the  $E_0$  conformer in favor of the accumulation of states that have received two and more electrons. In particular, the intensities of E<sub>4</sub>(4H) signals for WT enzyme are much less than those for α-V70I when freeze-trapped during Ar turnover under the modestly low electron flux ([Fe]/[MoFe]  $\sim 1$ ) that previously was used in order to achieve MoFe protein concentrations high enough for EPR and ENDOR study.8 This shows that it is HP-suppression in  $E_4(4H)$  of the α-V70I perturbed conformation that leads to freeze-trapping of E<sub>4</sub>(4H) in much higher occupancy ( $\sim$ 50% or greater) than for WT enzyme.

With such suppression of HP in  $\alpha$ -V70I, it can be inferred (i) that electrondelivery to the HP-inhibited conformation controls its accumulation of E<sub>4</sub>(4H), (ii) that the occupancy of the  $E_4(4H)$  state in the  $\alpha$ -V70I protein freeze quenched under Ar turnover is a rather faithful measure of the occupancy of the HPinhibited conformation at ambient temperatures, and (iii) that the interconversion between the conformers is slow, in keeping with the large activation energy calculated for interconversion. In principle, of course a conformational equilibrium will in general be temperature dependent, but this process is not altering the present measurements. Thus, electron delivery from the Fe protein to MoFe protein is relatively slow at ambient temperature, slows with cooling, and it is completely quenched on freezing the aqueous buffer solutions, which occurs not far below 0 °C. Therefore, during the rapid quench freezing of an aqueous-buffer enzyme solution in dry-ice/acetone or liquid nitrogen, it would be impossible to deliver enough electrons to MoFe to significantly increase the  $E_4(4H)$  occupancy as measured, and thus alter the inferred occupancies, while cooling would further slow interconversion.

#### E2(2H) states accumulated in turnover and during cryoannealing

Numerous intermediates have been freeze-trapped during turnover of WT and  $\alpha$ -V70I MoFe proteins, and cryoannealing measurements have been instrumental in determining the E<sub>n</sub>-state they represent. This subsection first describes the formation of E<sub>n</sub> states n = 2, 4 for WT and  $\alpha$ -V70I MoFe and phenomena observed during their cryoannealing, then analyzes their cryoannealing kinetics.

WT enzyme. When the electron flux is increased by decreasing the MoFe/Fe ratio from the extreme 100/1 value, but the flux nonetheless remains low

enough to keep the highly-reduced WT states  $E_3(3H)$  and  $E_4(4H)$  essentially depopulated, the most populated EPR-active intermediate trapped by freezequench of WT enzyme during turnover under Ar is the S=3/2 state with EPR signal of low rhombicity ( $g_1'=4.21,g_2'=3.76$ ), known as 1b.<sup>24</sup> The identification of the 1b signal with  $E_2(2H)$  had been made through the observation that during cryoannealing this signal directly converts into the  $E_0$  resting state signal 1a in a single step, with KIE  $\sim 3$  associated with the protonation of a hydride bound to the cofactor of  $E_2(2H)/1b$  with concomitant release of  $H_2$ .<sup>29</sup>

There is another S=3/2 conformer of the  $E_2(2H)$  state, with EPR signal of higher rhombicity,  $g'=[4.69,\,\sim 3.20,\,\sim 2]$  and historically named 1c.<sup>24</sup> In freeze-trapped WT turnover samples the 1c signal usually is even of lower amplitude than 1b, and is not easy to study. However its assignment to  $E_2(2H)$  was first indicated by the observation that 1c decays in a single step during cryoannealing, with relaxation characteristics similar to those of the  $E_2(2H)/1b$  relaxation.<sup>29</sup> The definitive assignment of 1c to an  $E_2(2H)$  state was achieved through photolysis experiments, which interconvert 1b and 1c, confirming that both signals arise from  $E_2(2H)$  conformers.<sup>33</sup>

Turnover of WT MoFe under substrate  $N_2$  allows freeze-trapping of  $E_4(2N2H)$ , the product of  $N_2$  binding/reduction coupled to  $H_2$  reductive elimination, Fig. 1. The identification of this state was established by cryoannealing, during which it relaxes in three steps. It oxidatively adds  $H_2$  and loses  $N_2$ , converting to  $E_4(4H)$ , which in turn converts in a single kinetic step with  $H_2$  loss to the  $E_2(2H)/1b$  state. This state decays more slowly than it is formed during cryoannealing, so it first accumulates (1b signal increases) before it in turn decays and converts to  $E_0/1a$  with  $H_2$  formation.8

α-V70I enzyme. The α-V70I variant was only studied under Ar turnover because its specific reactivity with  $N_2$  is much lower than WT. Under these conditions, freeze-trapping the α-V70I variant captures large populations of  $E_4(4H)$ ; no  $E_2(2H)$  state is trapped. As previously reported,  $^{12}$  and as shown in Fig. 7,  $^{12}$  cryoannealing relaxation of α-V70I  $E_4(4H)$  also proceeds to  $E_0$  in two steps, as with WT. However, during annealing, the α-V70I  $E_4(4H)$  state does not first relax to  $E_2(2H)$ /1b. Instead it relaxes to a 'high-rhombicity (hr)' S = 3/2 state,  $^{12}$  denoted  $E_2(2H)$ /hr, whose EPR signal has rhombicity ( $g'_1 = 5.26$ ,  $g'_2 = 2.58$ ) much greater than that of either the WT  $E_2(2H)$ /1b or 1c signals. As discussed below, this difference in the  $E_2(2H)$  state is ascribable to the presence of different isomers of the  $E_2(2H)$  hydride. Relaxation of α-V70I  $E_4(4H)$  through the  $E_2(2H)$ /hr intermediate primarily generates the mutation-perturbed  $E_0$ /1a′ resting state conformer. It is important to emphasize that this observation thus confirms that the high populations of  $E_4(4H)$  that accumulate during α-V70I turnover are associated with this perturbed conformer.

#### Cryoannealing relaxation schemes

In this subsection, we develop the schemes for the cryoannealing/relaxation of  $E_4(4H)$  and  $E_2(2H)$  (Fig. 1) of WT enzyme freeze-trapped during turnover under  $N_2$ , and of WT and  $\alpha$ -V70I MoFe freeze-trapped during turnover under Ar.

For the WT enzyme trapped during turnover under  $N_2$ , the cryoannealing process starts with the trapped diazene-level state  $E_4(2N2H)$  formed by the coupled binding of  $N_2$  and reductive elimination of  $H_2$  from the dihydride  $E_4(4H)$  during turnover (Fig. 1). During cryoannealing at -50 °C,  $E_4(2N2H)$ 

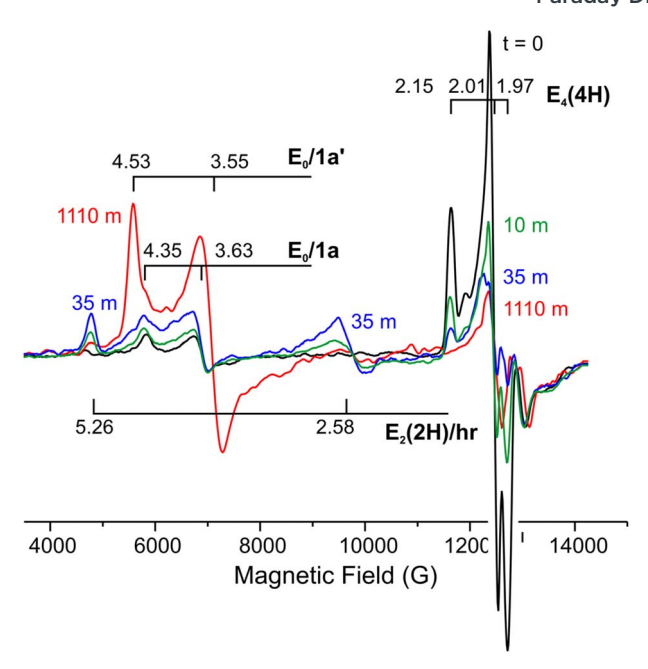
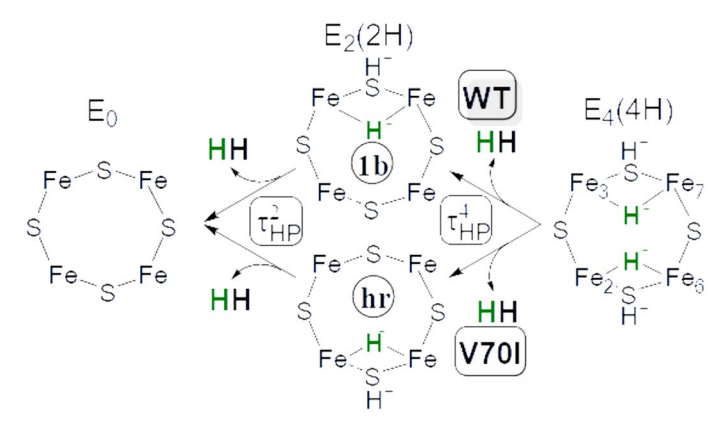


Fig. 7 Q-band T = 2 K EPR spectra taken at indicated times during 253 K cryoannealing of E<sub>4</sub>(4H) accumulated in  $\alpha$ -V70I Ar turnover: (0, 10, 35 and 1110 minutes). The figure is revised from ref. 12 to emphasize the subject of the current paper.

relaxes to the resting state  $E_0$  in three steps,<sup>8</sup> the first being oxidative addition of  $H_2$  and release of  $N_2$  to regenerate the  $E_4(4H)$  state. As visualized in Scheme 1, WT  $E_4(4H)$  then converts to  $E_2(2H)/1b$ , which in turn relaxes to  $E_0$ , with time constants listed in Table 1. Of particular note, the -50 °C cryoannealing process for WT enzyme exhibits a sharp,  $\sim$ 60-fold difference in the time constants for HP in  $E_4(4H)$  ( $\tau^4_{HP} \sim 6$ min) and in  $E_2(2H)$  ( $\tau^2_{HP} \sim 330$  min). It is this sharply



Scheme 1 Cryoannealing pathways for WT and  $\alpha$ -V70I nitrogenase. Labels on Fe ions of E<sub>4</sub>(4H) orient the view of the Fe2,3,6,7 face.

Table 1 Cryoannealing/relaxation time-constants (in minutes)

T	−50 °C		−20 °C	
Variant	$\mathrm{WT}^c$	V70I	WT	V70I <sup>d</sup>
$\tau^4_{\mathrm{HP}}{}^a$	6	≥600 <sup>f</sup>		13
$\tau^2_{\mathrm{HP}}{}^b$	330		~10 <sup>e</sup>	870

Estimates from stretched-exponential fits.
 Exponential fit.
 Ref. 8.
 Ref. 12.
 Unpublished.
 Estimated (see text). Note: arrows indicate HP time-constants assigned to Fe3–H–Fe7 (see text).

slower relaxation of  $E_2(2H)/1b$  compared to its formation that causes its buildup with subsequent slower decay during cryoannealing. The time constant for relaxation of WT  $E_2(2H)/1b$  to  $E_0$  at -20 °C also was measured, and found to be 30 times faster, Table 1.8,12

The  $\alpha$ -V70I  $E_4(4H)$  likewise relaxes to  $E_0$  in a two-step process that exhibits the buildup then decay of  $E_2(2H)$ , both steps exhibiting a KIE associated with HP and  $H_2$  release. However, although as noted above, the properties of the  $E_4(4H)$  state in  $\alpha$ -V70I are identical to those for WT MoFe, in perhaps the most dramatic consequence of the  $\alpha$ -V70I substitution, cryoannealing  $\alpha$ -V70I  $E_4(4H)$  does not produce the  $E_2(2H)/1b$  state formed during relaxation of WT  $E_4(4H)$ , but instead forms the high-rhombicity state  $E_2(2H)/hr$ , which accumulates then relaxes to  $E_0$ , Scheme 1.

The cryoannealing kinetics of the α-V70I variant also show a second remarkable consequence of the substitution: as anticipated above from the buildup of E<sub>4</sub>(4H) during turnover, both steps of E<sub>4</sub>(4H) relaxation through HP are dramatically slower than in the WT enzyme. Thus, during cryoannealing of  $\alpha$ -V70I E<sub>4</sub>(4H) at -50 °C, the temperature used for WT, relaxation was so slow that it was impracticable to carry out this process. Instead, to monitor the annealing process for α-V70I it was necessary to speed up the process by increasing the annealing temperature from -50 °C to -20 °C, and even at this more-elevated temperature the time constants for both annealing steps of  $\alpha$ -V70I are more than twice as large as for WT at -20 °C (Table 1). It should be noted that before choosing -20 °C for  $\alpha$ -V70I, lower temperatures were tested. With short 5 min annealing steps, no significant loss of the  $E_4(4H)$  signal intensity was observed for  $T \le -30$  °C, meaning that at each temperature, the time constant for  $E_4(4H) \rightarrow E_2(2H)$  conversion during cryoannealing of  $\alpha$ -V70I must be extremely large compared to that for WT. To put this in context, assuming we could not have detected a decrease in intensity of E4(4H) beyond reproducibility error in EPR recording (less than 5%) for 5 min at -50 °C, then the decay-time of  $E_4(4H)$  in  $\alpha$ -V70I at this temperature must be at least 100-fold greater than that for WT.

It thus appears that the two time constants for relaxation steps of  $E_4(4H)$  in  $\alpha$ -V70I are increased by comparable factors of ca. 100-fold compared to those for WT, accidentally keeping the  $\sim\!60$  fold difference between the time constants for the two steps observed for WT. However, as a foreshadowing that the situation will below prove to be more complex, the time-constant for the

second relaxation step in WT enzyme at -20 °C, namely  $\tau^2_{HP}(WT)$ , for the  $E_2(2H)/1b \rightarrow E_0$  relaxation, is essentially the same as that for the first hydride protonation in  $\alpha$ -V70I at -20 °C,  $\tau^4_{HP}$  ( $\alpha$ -V70I) for the relaxation,  $E_4(4H) \rightarrow E_2(2H)/hr$ , and this is likewise true for relaxation at -50 °C (see Table 1). These observations will be shown below to be arise because the influence of the  $\alpha$ -V70I substitution is to dramatically slow the HP of the Fe2–H–Fe6 hydride, strongly increasing its time-constant for HP at a given temperature without significant influence on the Fe3–H–Fe7 hydride, Table 1. Such an effect would cause the WT and  $\alpha$ -V70I variant to follow the alternative cryoannealing pathways as shown in Scheme 1, with the first step in the relaxation of  $E_4(4H)$  involving a different hydride in the two variants, Fe2–H–Fe6 in WT but Fe3–H–Fe7 in  $\alpha$ -V70I, and therefore with different products –  $E_2(2H)/1b$  in WT, but  $E_2(2H)/hr$  in  $\alpha$ -V70I.

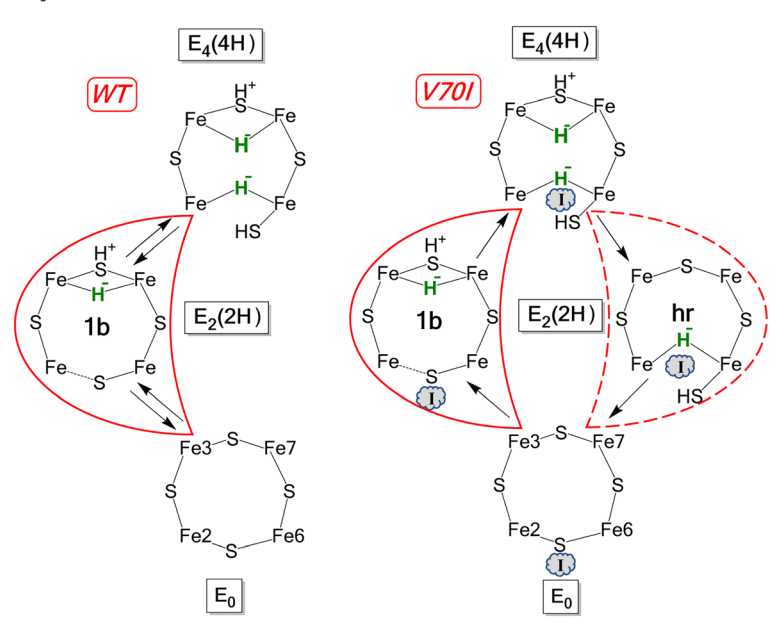
#### Implications of HP suppression for kinetic studies

As discussed above,  $N_2$  reduction in  $\alpha$ -V70I protein is diminished in comparison with that in WT enzyme because the large Ile sidechain blocks access of  $N_2$  to Fe6, showing that to be the  $N_2$  binding site, and not molybdenum. Trapping a high population of the  $E_4(4H)$  dihydride intermediate during turnover of  $\alpha$ -V70I, which enabled its detailed ENDOR study, was not expected, and came as a nice bonus. The cryoannealing results presented here demonstrate that accumulation of the  $E_4(4H)$  intermediate under Ar turnover of the substituted protein is enhanced because the substitution suppresses protonation of the Fe2–H–Fe6 hydride of  $E_4(4H)$ , while in doing so the substitution has altered the  $E_2(2H)$  state of the protein formed by HP of  $E_4(4H)$ . As a consequence of this, the enhanced accumulation of  $E_4(4H)$  seen in the  $\alpha$ -V70I enzyme relative to WT is only partially due to suppression of reaction with  $N_2$ , with a major contribution from suppressed HP at  $E_4(4H)$ .

The cryoannealing and the ambient-temperature, low-flux measurements (Fig. 6) agree in showing that the HP rate constants are sharply lower in the  $\alpha$ -V70I than in WT enzyme, an indication that the cryoannealing data is a faithful representation of the behavior at ambient. This in turn implies that the direct observation of an  $\sim$ 60-fold difference between rates for HP in E<sub>4</sub>(4H) and in E<sub>2</sub>(2H), as seen in cryoannealing of both WT enzyme and  $\alpha$ -V70I, likewise provides a faithful representation of the behavior at ambient. This conclusion represents a significant modification to the early conclusion based on analysis of previous pre-steady-state kinetic studies, that the HP rates for E<sub>4</sub>(4H) and E<sub>2</sub>(2H) of WT enzyme differ by less than a factor of two.¹

#### Structural interpretation of HP suppression in MoFe α-V70I

The formation of different  $E_2(2H)$  states during cryoannealing  $E_4(4H)$  of WT (1b) and of  $\alpha$ -V70I (hi-rhomb/hr), as well as the increased HP time constants seen during  $\alpha$ -V70I cryoannealing, can be explained jointly by two assumptions. First, that one of the two hydrides of  $E_4(4H)$ , which we will argue to be the Fe2–H–Fe6 hydride bridge in WT enzyme is intrinsically more reactive to HP than the other hydride, and therefore during relaxation of WT  $E_4(4H)$ , the Fe2–H–Fe6 selectively undergoes the initial HP reaction to release  $H_2$  and form the  $E_2(2H)/1b$  state containing the Fe3–H–Fe7 hydride, as shown in Schemes 1 and 2. Second, the  $\alpha$ -



Scheme 2 Pathways for formation and relaxation of  $E_4(4H)$  in WT and  $\alpha$ -V70I nitrogenase. Up arrows involve accumulation of  $2[e^-/H^+]$ ; down arrows involve  $H_2$  release. (View of Fe2.3.6.7 face as oriented in Scheme 1).

V70I substitution selectively inhibits the protonation of the Fe2–H–Fe6 hydride, to the extent that the highly accumulated  $E_4(4H)$  in the  $\alpha$ -V70I enzyme first releases  $H_2$  through the slow HP of the essentially unperturbed Fe3–H–Fe7 hydride of  $E_4(4H)$ , forming  $E_2(2H)/hr$ , which thus we conclude contains the Fe2–H–Fe6 hydride that has become stabilized to HP.

The observation that  $E_4(4H)$  exhibits identical EPR spectra in WT and  $\alpha$ -V70I enzymes indicates that reduction of  $N_2$  and other substrates in the  $\alpha$ -V70I MoFe variant is suppressed because this variant exhibits conformation(s) that passively block substrate access to the site of reaction, Fe6, rather than actively altering the reactivity of Fe6. The original report of the  $\alpha$ -V70I structure, analyzed in terms of a single Ile conformation, further considered two possible explanations for the increase in the time-constant for HP in  $E_4(4H)$  that causes the efficient trapping of  $E_4(4H)$  during Ar turnover of this variant.<sup>5</sup> Both explanations involve mutation-induced suppression of proton delivery to FeMo-co. One postulates the methyl group of isoleucine blocks protonation of the Fe2–H–Fe6 hydride by an  $H^+$  from  $\alpha$ -H195. In the other, the enlarged residue blocks  $H^+$  flow from waters adjacent to R-homocitrate. However, the  $E_4(4H)$  intermediate has two bridging hydrides, with each having an adjacent sulfur-bound proton available to protonate the hydride. Thus, additional proton delivery to the  $E_4(4H)$  form of FeMo-co from the active-site surroundings is unnecessary for HP.

Instead, QM computations now performed with the  $\alpha$ -V70I substitution strongly support a third explanation for how this modification enhances accumulation of E<sub>4</sub>(4H). As visualized above in Fig. 2, our previous computations<sup>9,34</sup> showed the bond between Fe2 and protonated S2B is hemilabile, and the Fe2–S2B

bond breaks to create a terminal Fe6–S2B–H sulfhydryl, which 'swings away' from its position in  $E_0$  (Fig. 8). <sup>35,36</sup> QM refinement of  $E_4$ (4H) in  $\alpha$ -V70I now indicates that Ile70 can adopt two conformations (Fig. 8), as observed for  $E_0$  (Fig. 4), with conformation 1 of  $E_4$ (4H) favored over conformation 2 by 25 kJ mol<sup>-1</sup> rather than only 5 kJ mol<sup>-1</sup> as in  $E_0$ .

Firstly, with the H-S2B sulfhydryl of E<sub>4</sub>(4H) 'swung out', the Ile sidechain of the dominant conformation 1 would not interact with it, in contrast to the interaction with bridging S2B in E<sub>0</sub>, offering an explanation for the absence of substitutioninduced changes in the properties of E<sub>4</sub>(4H), which are seen for E<sub>0</sub>. Secondly, and of perhaps greater importance, this offers the explanation for the substitutioninduced change in E<sub>4</sub>(4H) HP reactivity. The HP process for E<sub>4</sub>(4H) FeMo-co containing the Fe-S2B-H fragment must involve rotation of the S2B-H back towards Fe2, to bring the H<sup>+</sup> on sulfur into contact with the Fe2-H-Fe6 hydride, and computations by Thorhallsson and Bjornsson indicate the same situation occurs for HP of this hydride in the E<sub>2</sub>(2H) state.<sup>37</sup> However, given the conformational flexibility of the Ile side chain proximate to Fe6 in the crystal of restingstate  $\alpha$ -V70I, Fig. 4, we propose that in E<sub>4</sub>(4H) the sidechain adopts a conformation that is a variant of conformation 1 of Fig. 4, in which its  $C_{\delta 1}$  methyl group sterically, but passively, blocks the repositioning of the S2B-H sulfhydryl (transient re-formation of the Fe6-S2B bond) that precedes protonation of Fe2-H-Fe6 by the S2B proton. This passive blocking, illustrated in Scheme 2, can be viewed as analogous to the sidechain's passive blocking of the approach of N2 to Fe6, and would not create substitution-induced changes in the properties of  $E_4(4H)$ .

We propose it is this steric obstruction that causes the time-constant for HP of hydride Fe2–H–Fe6 during cryoannealing to increase dramatically from its value in WT enzyme, becoming roughly 60-fold longer than for HP of the Fe3–H–Fe7 hydride, and leading to a lengthening of the time-constant for HP of Fe2–H–Fe6 by 3 to 4 orders of magnitude. Such a decrease in reactivity would make this

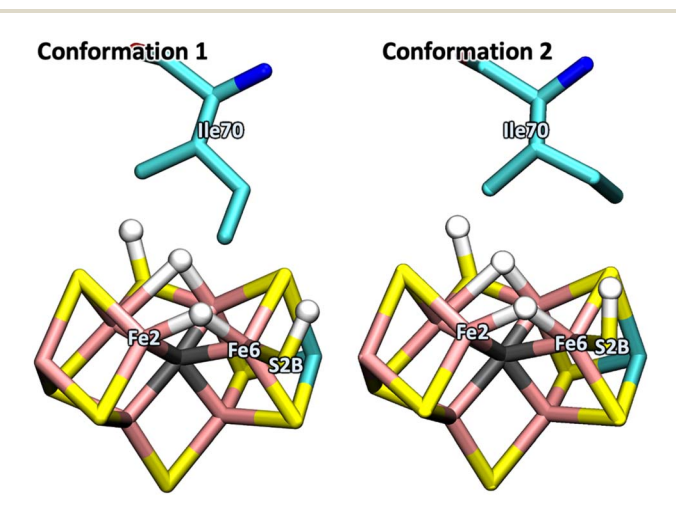


Fig. 8 Structure of  $E_4(4H)$  in the  $\alpha$ -V70I variant with Ile conformers 1 (left) and 2 (right) at the Ile position as obtained from density functional theory calculations. The FeMo-co atoms are colored as follows: sulfurs in yellow, central carbide in dark gray, irons in rust, and Mo in teal.

conformation effectively unreactive to HP, thereby enabling the buildup of  ${\rm E_4(4H)}$  seen with freeze–quench.

This analysis in turn implies that the first step in cryoannealing  $E_4(4H)$  trapped in the HP-suppressed conformation of the  $\alpha$ -V70I variant, denoted  $E_4(4H)_I$ , is protonolysis of the Fe3–H–Fe7 hydride, with a time constant largely unchanged by the substitution from that of the second HP of WT, Scheme 2 and Table 1. This creates the  $E_2(2H)$ /hr conformer that retains the Fe2–H–Fe6 hydride, not  $E_2(2H)$ /1b as forms by relaxation in WT enzyme. The Fe2–H–Fe6 hydride eventually undergoes its sterically-hindered, slow HP with release of  $H_2$ , probably enabled by repositioning of the Ile sidechain, returning the enzyme to the  $E_0$  state.

This proposal not only identifies hydride Fe2–H–Fe6 as undergoing the first hydride protonation of WT  $E_4(4H)$ , Scheme 2; it further identifies the  $E_2(2H)/1b$  state, which is both trapped during turnover and produced by cryoannealing/ relaxation of WT  $E_4(4H)$ , as containing the bridging Fe3–H–Fe7 hydride. In short this proposal for the behavior of the  $\alpha$ -V70I variant implies that electron/ proton accumulation by WT nitrogenase proceeds through initial formation of  $E_2(2H)/1b$ , with a Fe3–H–Fe7 hydride bridge. Hydride fluxionality at ambient temperatures could well lead to a dynamic partial hydride transfer to Fe2/Fe6 in  $E_2(2H)$ , but the trapping of the 1b signal both during turnover and during cryoannealing/relaxation of  $E_4(4H)$  indicates that  $E_2(2H)/1b$ , which has the Fe3–H–Fe7 hydride bridge, is the preferred form. Subsequent accumulation of two additional  $[e^-/H^+]$  then leads to formation of  $E_4(4H)$  with hydrides bridging both Fe3/Fe7 and Fe2/Fe6.

Obstruction by the  $C_{\delta 1}$  methyl group of the Ile substituent likewise explains hindered HP in  $\alpha$ -V70I if one instead favors either of the two lowest-energy  $E_4(4H)$  structures of Cao and Ryde. In both of these the Fe2–S2B–Fe6 bridge remains intact, and the two bridging hydrides are each flanked by a bridging SH (Fig. 9). However, in their state with parallel bridging hydrides, the adjacent S–H proton is directed 'away' from the hydride. The SH group thus must still 'reorganize' to bring the nascent  $H^+$  in contact with the hydride, and again the Ile  $C_{\delta 1}$  methyl could sterically hinder the reorganization. These considerations however do provide an argument against their alternative, slightly more-stable structure, in which the  $C_{\delta 1}$  methyl group would not be likely to hinder protonation (Fig. 9). Finally, if one considers the extreme possibility that S2B is actually released from

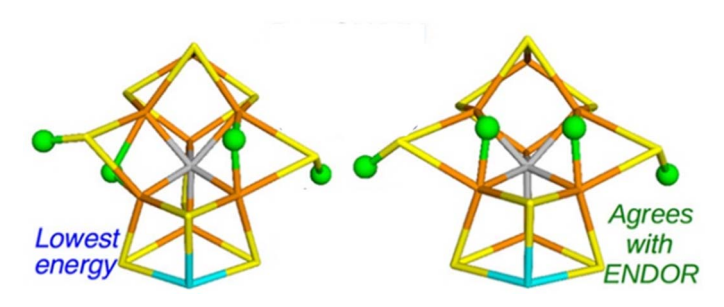


Fig. 9 Best QM/MM structures of  $E_4$ (4H) have two bridging hydrides, from report by, and with figure adapted from ref. 36. Fe atoms are colored rust, S atoms yellow, H atoms green, Mo atom teal, and C atom gray. The calculated lowest energy state is shown on the left and the proposed structure from ENDOR on the right.

FeMo-co in  $E_4(4H)$ , <sup>36</sup> passive hindrance to its return could explain suppression of HP by the Ile sidechain.

Formation of E<sub>4</sub>(2H)\* during Ar turnover of α-V70I protein. An unexpected consequence of the α-V70I substitution is the appearance of an EPR signal whose g-values, g = [2.11, 2.01, 1.96], Fig. 10, are characteristic of the state denoted E<sub>4</sub>(2H)\*.<sup>39</sup> The signal is always minor and its intensity varies with preparation of the freeze quenched α-V70I turnover sample. As an example, Fig. 10 compares spectra from two turnover samples that clearly show the features of the E<sub>4</sub>(2H)\* signal. The ESI† presents evidence confirming that the signal represents E<sub>4</sub>(2H)\* accumulated in low occupancy during turnover of α-V70I.

Formation of  $E_4(2H)^*$  state would occur upon the direct reductive elimination of  $H_2$  from  $E_4(4H)$  uncoupled from  $N_2$  binding, leaving the two remaining electrons accumulated by  $E_4(4H)$  as having doubly-reduced the FeS core of FeMo-co, with the two associated protons bound to sulfur, Scheme S1.†<sup>34,39,40</sup> Previously, the  $E_4(2H)^*$  state was only seen upon photolysis of WT  $E_4(4H)^*$ , it is never observed during WT turnover under any atmosphere, neither Ar or  $N_2$ . In particular, this

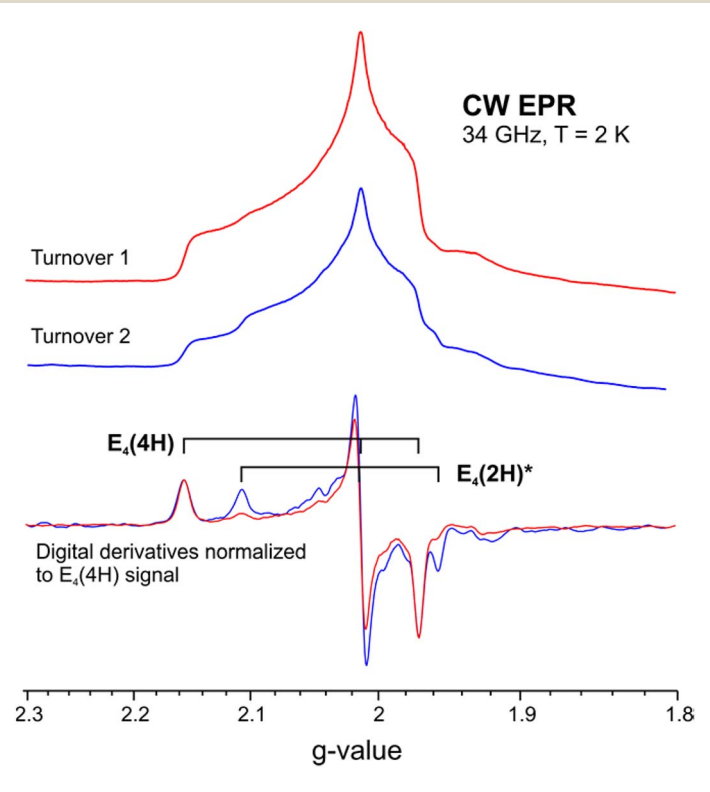


Fig. 10 CW, absorption-display rapid passage EPR spectra of two states of the same  $\alpha$ -V70I  $D_2O$  sample trapped during turnover. 'Turnover 1', as trapped; 'Turnover 2', which shows increased population of  $E_4(2H)^*$ , was prepared after complete annealing at -20 °C (1110 min), followed by turnover for 15 seconds at +30 °C. The digital derivatives of the spectra (low) were normalized to  $E_4(4H)$  signal amplitude for assignment of the state raised in 'Turnover 2'. EPR conditions: temperature, 2 K; microwave frequency,  $\sim$ 35 GHz; microwave power, 0.32 mW; modulation amplitude, 4 G; time constant, 128 ms; 4 minutes field scans.

$$E_{2}(2H)$$
 $E_{4}(4H)$ 
 $E_{4}(2H)^{*}$ 
 $E_{4}(2H)^{}$ 

Scheme 3 Formation of E<sub>4</sub>(2H)\*.

state from  $E_4(4H)$  does not play any role in WT turnover under  $N_2$ , as explained directly below.

Why would  $E_4(2H)^*$  form during Ar turnover of  $\alpha$ -V70I, but not WT turnover? As indicated in Scheme 3, direct hydride reductive elimination from  $E_4(4H)$  to form  $E_4(2H)^*$  must occur in kinetic competition with hydride protonation. The observation that  $\alpha$ -V70I under Ar turnover exhibits even a low level of re from  $E_4(4H)_I$  to form  $E_4(2H)^*$  (Fig. 10) thus implies that in the WT enzyme this process is kinetically outcompeted by the far more rapid hydride protonation of  $E_4(4H)$ . In short, it appears that in the HP-suppressed  $\alpha$ -V70I conformation that accumulates a high population of  $E_4(4H)$  the time constant for HP is increased to such an extent that  $E_4(2H)^*$  can accumulate to very low, but observable levels.

# Summary

The present measurements show that the  $\alpha$ -V70I substitution creates two types of active-site conformations in the resting-state (E<sub>0</sub>) enzyme, as visualized by reanalysis of the  $\alpha$ -V70I crystal structure and QM computations, Fig. 4. The measurements as supported by computations further suggest accumulation of E<sub>4</sub>(4H) is enhanced in  $\alpha$ -V70I because this state exhibits sidechain conformation(s) in which steric hindrance by the isoleucine C<sub>\delta1</sub> passively blocks protonation of the Fe2–H-Fe6 hydride by the proton on S2B (Scheme 2). Prior DFT computations of E<sub>4</sub>(4H) indicate that the Fe2–S2B bond in this state is hemilabile and breaks to form an Fe6–S2B–H sulfhydryl that 'swings away' from the cofactor (Fig. 2), while the current QM computations of the E<sub>4</sub>(4H) state identify a dominant Ile conformer, Fig. 8, in which we propose that the Ile C<sub>\delta1</sub> blocks the 'swingback' of the Fe6–S2B–H and Fe2–S2B rebinding necessary to bring the sulfhydryl proton and hydride in proximity for HP as visualized in Scheme 2. As an alternative possibility, based on computations of Cao and Ryde, C<sub>\delta1</sub> blocks

repositioning of the proton on an intact Fe2–SH–Fe6 moiety, Fig. 9. As a result of the steric interference inferred for either model, the time-constant for spontaneous protonation of the Fe2–H–Fe6 hydride, as measured during  $E_4(4H)$  cryoannealing, is increased by 3 to 4 orders of magnitude, thereby changing the order in which the two hydrides are protonated on the 2-step cryoannealing relaxation pathway to  $E_0$  (Scheme 2).

As further visualized in Scheme 2, both WT and  $\alpha$ -V70I variant accumulate four electrons to form the E<sub>4</sub>(4H) Janus intermediate (Fig. 1) through a pathway that leads through the doubly-reduced E<sub>2</sub>(2H)/1b intermediate, which stores its two accumulated electrons as an Fe3–H–Fe7 hydride bridge, then proceeds to form E<sub>4</sub>(4H), with two hydride bridges, Fe3–H–Fe7 and Fe2–H–Fe6. During relaxation of E<sub>4</sub>(4H) in WT enzyme, HP of Fe2–H–Fe6 forms E<sub>2</sub>(2H)/1b, which contains Fe3–H–Fe7; in E<sub>4</sub>(4H) of  $\alpha$ -V70I, HP of Fe3–H–Fe7 forms E<sub>2</sub>(2H)/hr, which contains Fe2–H–Fe6, Scheme 2.

The suppression of HP in the  $E_4(4H)$  state of  $\alpha$ -V70I by passive sidechain obstruction, as schematized in Scheme 2, is then responsible for the ability to freeze-trap a high population of this state unperturbed by the substitution, with the resulting EPR/ENDOR/photolysis characterization of this state that has played a central role in current understanding of the nitrogenase catalytic mechanism. In addition, it now appears that by strongly slowing HP at the  $E_4$  stage, the  $\alpha$ -V70I substitution slightly unmasks a third reaction channel for the  $E_4(4H)$  Janus intermediate that is entirely precluded by rapid HP during turnover of WT enzyme: the first-order reductive elimination of  $H_2$  without  $N_2$  binding/reduction, to form  $E_4(2H)^*$  (Scheme 3).

### **Author contributions**

All authors contributed to the investigation: D. R. D. for genetics and strain construction, Z. Y. Y. for protein purification and sample preparation, D. A. L. for collection of all spectra, D. A. L. and B. M. H. for spectra interpretation, K. S. and J. W. P. for X-ray crystallography, S. R. for calculations. B. M. H., D. A. L., and L. C. S. wrote the original draft. All authors contributed to review and editing.

## Conflicts of interest

There are no conflicts to declare.

## Acknowledgements

Spectroscopy work was supported by the U.S. National Science Foundation (MCB-1908587, B. M. H.). Clone construction, sample preparation, and X-ray structure determination was supported by the U.S. Department of Energy (DOE), Office of Science, Office of Basic Energy Sciences (DE-SC0010687, DE-SC0010834, DE-SC0018143 to L. C. S., D. R. D., J. W. P.). S. R. did calculations with support provided by the U.S. DOE, Office of Science, Office of Basic Energy Sciences, Division of Chemical Sciences, Geosciences, and Biosciences. Computer time was provided by the National Energy Research Scientific Computing Center (NERSC), a U.S. DOE Office of Science User Facility operated by Lawrence Berkeley National Laboratory, and the Molecular Sciences Computing Facility (MSCF) in the

Environmental Molecular Sciences Laboratory, a DOE User Facility located at the Pacific Northwest National Laboratory (PNNL). PNNL is operated by Battelle for the DOE under Contract number DE-AC05-76RL01830.

## References

- 1 B. K. Burgess and D. J. Lowe, Mechanism of Molybdenum Nitrogenase, *Chem. Rev.*, 1996, **96**, 2983–3012.
- 2 B. M. Hoffman, D. Lukoyanov, Z. Y. Yang, D. R. Dean and L. C. Seefeldt, Mechanism of Nitrogen Fixation by Nitrogenase: The Next Stage, *Chem. Rev.*, 2014, 114, 4041–4062.
- 3 L. C. Seefeldt, Z. Y. Yang, D. A. Lukoyanov, D. F. Harris, D. R. Dean, S. Raugei and B. M. Hoffman, Reduction of Substrates by Nitrogenases, *Chem. Rev.*, 2020, 120, 5082–5106.
- 4 B. M. Barney, R. Y. Igarashi, P. C. Dos Santos, D. R. Dean and L. C. Seefeldt, Substrate Interaction at an Iron–Sulfur Face of the FeMo-Cofactor During Nitrogenase Catalysis, *J. Biol. Chem.*, 2004, **279**, 53621–53624.
- 5 R. Y. Igarashi, P. C. Dos Santos, W. G. Niehaus, I. G. Dance, D. R. Dean and L. C. Seefeldt, Localization of a Catalytic Intermediate Bound to the FeMo-Cofactor of Nitrogenase, *J. Biol. Chem.*, 2004, 279, 34770–34775.
- 6 R. Y. Igarashi, M. Laryukhin, P. C. Dos Santos, H. I. Lee, D. R. Dean, L. C. Seefeldt and B. M. Hoffman, Trapping H<sup>-</sup> Bound to the Nitrogenase FeMo-Cofactor Active Site During H<sub>2</sub> Evolution: Characterization by ENDOR Spectroscopy, *J. Am. Chem. Soc.*, 2005, 127, 6231–6241.
- 7 V. Hoeke, L. Tociu, D. A. Case, L. C. Seefeldt, S. Raugei and B. M. Hoffman, High-Resolution ENDOR Spectroscopy Combined with Quantum Chemical Calculations Reveals the Structure of Nitrogenase Janus Intermediate E<sub>4</sub>(4H), J. Am. Chem. Soc., 2019, 141, 11984–11996.
- 8 D. Lukoyanov, N. Khadka, Z. Y. Yang, D. R. Dean, L. C. Seefeldt and B. M. Hoffman, Reductive Elimination of  $H_2$  Activates Nitrogenase to Reduce the N $\equiv$ N Triple Bond: Characterization of the  $E_4(4H)$  Janus Intermediate in Wild-Type Enzyme, *J. Am. Chem. Soc.*, 2016, **138**, 10674–10683.
- 9 S. Raugei, L. C. Seefeldt and B. M. Hoffman, Critical Computational Analysis Illuminates the Reductive-Elimination Mechanism That Activates Nitrogenase for  $N_2$  Reduction, *Proc. Natl. Acad. Sci. U. S. A.*, 2018, 115, E10521–E10530.
- 10 B. M. Barney, D. Lukoyanov, R. Y. Igarashi, M. Laryukhin, T. C. Yang, D. R. Dean, B. M. Hoffman and L. C. Seefeldt, Trapping an Intermediate of Dinitrogen (N<sub>2</sub>) Reduction on Nitrogenase, *Biochemistry*, 2009, 48, 9094–9102.
- 11 D. Lukoyanov, Z. Y. Yang, N. Khadka, D. R. Dean, L. C. Seefeldt and B. M. Hoffman, Identification of a Key Catalytic Intermediate Demonstrates That Nitrogenase Is Activated by the Reversible Exchange of N<sub>2</sub> for H<sub>2</sub>, *J. Am. Chem. Soc.*, 2015, 137, 3610–3615.
- 12 D. Lukoyanov, B. M. Barney, D. R. Dean, L. C. Seefeldt and B. M. Hoffman, Connecting Nitrogenase Intermediates with the Kinetic Scheme for  $N_2$  Reduction by a Relaxation Protocol and Identification of the  $N_2$  Binding State, *Proc. Natl. Acad. Sci. U. S. A.*, 2007, **104**, 1451–1455.
- 13 J. Christiansen, P. J. Goodwin, W. N. Lanzilotta, L. C. Seefeldt and D. R. Dean, Catalytic and Biophysical Properties of a Nitrogenase Apo-MoFe Protein

- Produced by a *nifB*-Deletion Mutant of *Azotobacter vinelandii*, *Biochemistry*, 1998, 37, 12611–12623.
- 14 M. M. Georgiadis, H. Komiya, P. Chakrabarti, D. Woo, J. J. Kornuc and D. C. Rees, Crystallographic Structure of the Nitrogenase Iron Protein from Azotobacter vinelandii, Science, 1992, 257, 1653–1659.
- 15 S. Stoll and A. Schweiger, EasySpin, a Comprehensive Software Package for Spectral Simulation and Analysis in EPR, J. Magn. Reson., 2006, 178, 42–55.
- 16 M. M. Werst, C. E. Davoust and B. M. Hoffman, Ligand Spin Densities in Blue Copper Proteins by Q-band Proton and Nitrogen-14 ENDOR Spectroscopy, *J. Am. Chem. Soc.*, 1991, 113, 1533–1538.
- 17 C. E. Davoust, P. E. Doan and B. M. Hoffman, Q-Band Pulsed Electron Spin-Echo Spectrometer and Its Application to ENDOR and ESEEM, *J. Magn. Reson., Ser. A*, 1996, **119**, 38–44.
- 18 D. Smith, K. Danyal, S. Raugei and L. C. Seefeldt, Substrate Channel in Nitrogenase Revealed by a Molecular Dynamics Approach, *Biochemistry*, 2014, 53, 2278–2285.
- 19 A. D. Becke, Density-Functional Exchange-Energy Approximation with Correct Asymptotic Behavior, *Phys. Rev. A: At., Mol., Opt. Phys.*, 1988, 38, 3098–3100.
- 20 J. P. Perdew, Density-Functional Approximation for the Correlation Energy of the Inhomogeneous Electron Gas, *Phys. Rev. B: Condens. Matter Mater. Phys.*, 1986, 33, 8822–8824.
- 21 J. P. Perdew, Erratum: Density-Functional Approximation for the Correlation Energy of the Inhomogeneous Electron Gas, *Phys. Rev. B: Condens. Matter Mater. Phys.*, 1986, 34, 7406.
- 22 F. Weigend and R. Ahlrichs, Balanced Basis Sets of Split Valence, Triple Zeta Valence and Quadruple Zeta Valence Quality for H to Rn: Design and Assessment of Accuracy, *Phys. Chem. Chem. Phys.*, 2005, 7, 3297–3305.
- 23 M. Dolg, H. Stoll and H. Preuss, Energy-Adjusted *Ab Initio* Pseudopotentials for the Rare Earth Elements, *J. Chem. Phys.*, 1989, **90**, 1730–1734.
- 24 D. J. Lowe, R. R. Eady and N. F. Thorneley, Electron-Paramagnetic-Resonance Studies on Nitrogenase of Klebsiella pneumoniae. Evidence for Acetylene- and Ethylene-Nitrogenase Transient Complexes, *Biochem. J.*, 1978, 173, 277–290.
- 25 R. J. Gurbiel, J. T. Bolin, A. E. Ronco, L. Mortenson and B. M. Hoffman, Single-Crystal EPR and ENDOR Study of Nitrogenase from *Clostridium pasteurianum*, *J. Magn. Reson.*, 1991, 91, 227–240.
- 26 T. Spatzal, O. Einsle and S. L. A. Andrade, Analysis of the Magnetic Properties of Nitrogenase FeMo Cofactor by Single-Crystal EPR Spectroscopy, *Angew. Chem., Int. Ed.*, 2013, 52, 10116–10119.
- 27 D. Lukoyanov, Z.-Y. Yang, D. R. Dean, L. C. Seefeldt and B. M. Hoffman, Is Mo Involved in Hydride Binding by the Four-Electron Reduced (E<sub>4</sub>) Intermediate of the Nitrogenase MoFe Protein?, *J. Am. Chem. Soc.*, 2010, **132**, 2526–2527.
- 28 A. E. True, P. McLean, M. J. Nelson, W. H. Orme-Johnson and B. M. Hoffman, Comparison of Wild-Type and nifV Mutant Molybdenum-Iron Proteins of Nitrogenase from Klebsiella-pneumoniae by ENDOR Spectroscopy, *J. Am. Chem. Soc.*, 1990, 112, 651–657.
- 29 D. Lukoyanov, Z. Y. Yang, S. Duval, K. Danyal, D. R. Dean, L. C. Seefeldt and B. M. Hoffman, A Confirmation of the Quench-Cryoannealing Relaxation Protocol for Identifying Reduction States of Freeze-Trapped Nitrogenase Intermediates, *Inorg. Chem.*, 2014, 53, 3688–3693.

- 30 K. Danyal, S. Shaw, T. R. Page, S. Duval, M. Horitani, A. R. Marts, D. Lukoyanov, D. R. Dean, S. Raugei, B. M. Hoffman, L. C. Seefeldt and E. Antony, Negative Cooperativity in the Nitrogenase Fe Protein Electron Delivery Cycle, *Proc. Natl. Acad. Sci. U. S. A.*, 2016, 113, E5783–E5791.
- 31 R. N. F. Thorneley and D. J. Lowe, Kinetics and Mechanism of the Nitrogenase Enzyme System, *Met. Ions Biol.*, 1985, 7, 221–284.
- 32 K. Fisher, D. J. Lowe and R. N. F. Thorneley, Klebsiella pneumoniae Nitrogenase. The Pre-Steady-State Kinetics of MoFe-Protein Reduction and Hydrogen Evolution under Conditions of Limiting Electron Flux Show That the Rates of Association with the Fe-Protein and Electron Transfer Are Independent of the Oxidation Level of the MoFe-Protein, *Biochem. J.*, 1991, 279, 81–85.
- 33 D. A. Lukoyanov, N. Khadka, Z. Y. Yang, D. R. Dean, L. C. Seefeldt and B. M. Hoffman, Hydride Conformers of the Nitrogenase FeMo-Cofactor Two-Electron Reduced State E<sub>2</sub>(2H), Assigned Using Cryogenic Intra Electron Paramagnetic Resonance Cavity Photolysis, *Inorg. Chem.*, 2018, 57, 6847–6852.
- 34 D. A. Lukoyanov, Z. Y. Yang, D. R. Dean, L. C. Seefeldt, S. Raugei and B. M. Hoffman, Electron Redistribution within the Nitrogenase Active Site FeMo-Cofactor During Reductive Elimination of H₂ to Achieve N≡N Triple-Bond Activation, *J. Am. Chem. Soc.*, 2020, 142, 21679–21690.
- 35 We note an alternative, more extensive modification has been considered, in which the H-S2B sulfhydryl actually is lost during the catalytic cycle and regained by its end.
- 36 O. Einsle and D. C. Rees, Structural Enzymology of Nitrogenase Enzymes, Chem. Rev., 2020, 120, 4969–5004.
- 37 A. T. Thorhallsson and R. Bjornsson, The E<sub>2</sub> State of FeMoco: Hydride Formation *versus* Fe Reduction and a Mechanism for H<sub>2</sub> Evolution, *Chem. Eur. J.*, 2021, 27, 16788–16800.
- 38 L. Cao and U. Ryde, What Is the Structure of the E<sub>4</sub> Intermediate in Nitrogenase?, *J. Chem. Theory Comput.*, 2020, **16**, 1936–1952.
- 39 D. Lukoyanov, N. Khadka, Z. Y. Yang, D. R. Dean, L. C. Seefeldt and B. M. Hoffman, Reversible Photoinduced Reductive Elimination of H<sub>2</sub> from the Nitrogenase Dihydride State, the E<sub>4</sub>(4H) Janus Intermediate, *J. Am. Chem. Soc.*, 2016, **138**, 1320–1327.
- 40 D. Lukoyanov, N. Khadka, D. R. Dean, S. Raugei, L. C. Seefeldt and B. M. Hoffman, Photoinduced Reductive Elimination of H<sub>2</sub> from the Nitrogenase Dihydride (Janus) State Involves a FeMo-Cofactor-H<sub>2</sub> Intermediate, *Inorg. Chem.*, 2017, 56, 2233–2240.